

Topological analysis of brain dynamical signals reveals signatures of seizure susceptibility

Maxime Lucas,^{1,2} Damien Francois,^{3,4} Cristina Donato,⁴ Alexander Skupin,^{4,5,6} and Daniele Proverbio⁷

¹*Department of Mathematics & Namur Institute for Complex Systems (naXys), Université de Namur, Namur, Belgium*

²*CENTAI Institute, Turin, Italy*

³*Interdisciplinary Centre for Security, Reliability and Trust; University of Luxembourg; 29, Avenue J.F Kennedy, 1855; Luxembourg*

⁴*Luxembourg Centre for Systems Biomedicine; University of Luxembourg; Belvaux, 6 Avenue du Swing, 4367; Luxembourg*

⁵*Department of Physics and Material Science ; University of Luxembourg; Luxembourg, 162a, avenue de la Faiënerie, 1511; Luxembourg*

⁶*National Center for Microscopy and Imaging Research; University of California San Diego; La Jolla, Gilman Drive, CA, 9500; United States*

⁷*Department of Industrial Engineering; University of Trento; Trento, 9 via Sommarive, 38123; Italy*

Epilepsy is known to drastically alter brain dynamics during seizures (ictal periods). However, whether epilepsy may alter brain dynamics during background (non-ictal) periods is less understood. To investigate this, we analyzed the brain activity of epileptic zebrafish as animal models, for two genetic conditions and two fishlines. The recordings were automatically segmented and labeled with machine learning, and then analyzed using Persistent Homology, a method from Topological Data Analysis, which reveals patterns in the topology of brain dynamics in a noise-robust and network-based manner. We find that ictal and non-ictal periods can be distinguished from the topology of their dynamics, regardless of fishline or genetic condition, which validates our method. Additionally, within a single fishline wild type, we can distinguish the non-ictal periods of seizure-prone and seizure-free individuals. This suggests the presence of topological signatures of the epileptic brain, even during non-ictal periods. In general, our results suggest that Topological Data Analysis can be used as a general quantitative method to screen for dynamical markers of seizure susceptibility also in other species.

I. INTRODUCTION

Epilepsy, a neurological disorder affecting approximately 50 million people worldwide [1], is characterized by recurring seizures (ictal periods) that disrupt normal brain activity. It is a complex and multifaceted disorder that demands interdisciplinary research to understand its causes and mechanisms, develop effective monitoring and treatment strategies, and eventually improve patients' outcomes. In particular, for patients with established epilepsy, predicting or detecting seizures using time-series recordings is critical. Advances in wearable devices have enabled continuous monitoring of brain activity, and algorithms based on signal processing [2] or machine learning [3] can now identify seizures. In addition, studies have modeled seizure onset using detailed dynamical frameworks capable of reproducing common seizure patterns across diverse epilepsy types [4], and revealed cyclic rhythms in seizures [5].

On longer time scales, a lasting challenge is to detect susceptibility to develop epilepsy in non-ictal brains. Biological markers and conditions such as strokes, head injuries, or brain tumors, may suggest higher risk of developing seizures, but they account for about 25% of the cases [6]. Genetic studies have advanced the classification of some causes and identified genes related to epilepsy propensity [6], but require extensive screening and do not integrate information about brain dynamics. Taking the standpoint of the analysis of brain activity, a key open question in epileptogenesis studies is, whether non-ictal

brain dynamics can reveal signatures of seizure susceptibility. A positive answer would open new avenues for monitoring and detection of latent epileptic conditions, and foster the integration of biological blueprints with the analysis of dynamical systems. Hence, we address it by systematically analyzing brain activity of a curated dataset, under the lenses of dynamical systems methods.

From a dynamical systems perspective [7], brain activity can be viewed as the output of a high-dimensional system, organized into dynamical attractors corresponding to distinct brain states (e.g., seizures or background activity). Several attractors can coexist and transitions between them are triggered by internal or external stimuli [8–10]. The size of an attractor's basin of attraction reflects its “attractiveness” and resilience [11]; the larger it is, the more likely the system will end up in that attractor and the less likely it will leave it. In this framework, seizures can be viewed as dynamics within a dynamical attractor, with the frequency of seizure occurrence being linked to the basin size [12]. This perspective provides one way of explaining why diverse biological mechanisms—including genetic, infectious, metabolic, or immune factors [6]—are associated with epileptogenesis: various conditions can concur to shape similar attractor dynamics, destabilizing the “healthy” attractor and making the seizure attractor more reachable [13, 14].

An important aspect of dynamical attractors is their topology, which quantifies properties such as shape or the presence of repeated patterns. Topological Data Analysis (TDA), as its name suggests, is a field that provides

tools to study the topology (or shape) of datasets and time-series recordings. TDA is robust to noise and scale resolution [15–17], and fully captures non-linear features of dynamical attractors [18], providing more rich information than other methods based on signal processing and state-space reconstruction [19–21]. Moreover, it is interpretable thanks to its underlying mathematical theory, thus overcoming the shortcomings summary statistics, machine- and deep-learning [3, 22, 23]. TDA is thus well-suited for high-dimensional data, and enables quantitative comparison of topological features often invisible to traditional methods like recurrence analysis or time-frequency analysis. Overall, in combination with time-delay embedding [24], TDA can aptly reconstruct and analyze the topology of attractors from time series, which have made TDA increasingly popular in neuroscience [25–32] as well as other fields like physiology or finance [33–35].

Although TDA has been applied to epilepsy in a handful of studies, they have focused mainly on seizure detection [26, 29, 36]. These studies, often based on clinical patient datasets, suffer from limited control over biological conditions and may lack control cohorts. To address these limitations, animal models of epilepsy have been developed [37, 38], providing reproducible and controlled conditions for both microbiological studies and time-series analysis [39, 40]. Zebrafish (*Danio rerio*) have emerged as a valuable model organism for epilepsy research and translational research in particular [41, 42]. Epileptic susceptibility in zebrafish larvae can arise from genetic mutations or be pharmacologically induced using convulsant drugs. In addition, brain activity can be monitored using local field potential (LFP) recordings [43], and precise knowledge of genetic profiles and laboratory conditions supports the establishment of high-quality curated and labeled datasets.

In this study, we aim to quantitatively characterize dynamical seizure susceptibility, identifying its signatures from time-series of brain activity, subject to various biological conditions. To this end, we use an in-house Zebrafish dataset of local field potential (LFP) recordings, measured during seizures and background activity from two fishlines, each one represented by a wild type and by a controlled genetic mutation. To characterize the topology of the dynamical attractor associated to each recording, we used three topological metrics from TDA—total persistence, persistent entropy, and persistent Betti numbers [44]. First, we validated the method by showing that these topological metrics can discriminate between seizures and background, regardless of fishline and genetic condition. Second, we found that they cannot distinguish between fishlines except for a specific case: background activity of mutants, by looking at the homological dimension 1. This suggests some common topological features of the dynamics between fishlines. Finally, we showed that within a single fishline, individuals that have had seizures, and are prone to develop new ones, can be distinguished from those who have not,

solely based on the topology of their dynamics. These findings suggest that TDA has the potential to significantly contribute to the detection and characterization of epileptic states, and open to the possibility of inferring signatures of seizure susceptibility by looking for altered dynamical landscapes.

II. RESULTS

A. Experimental Data

Experiments were carried out on two epileptogenic fishlines that carry mutations (MUT) in either *ash1l* or *kcnq5a* genes, as well as their wild-type (WT) variants. All strains can exhibit seizure and non-seizure events. Local field potential (LFP) was recorded with a single electrode per fish (Fig. 1a). After segmenting the LFP recordings and labeling them, each time series is thus associated with a triplet (Fishline, Condition, Event), where each entry can take two values ($\{\text{kcnq5a}; \text{ash1l}\}$, $\{\text{MUT}; \text{WT}\}$, $\{\text{background}; \text{seizure}\}$). In addition, we benchmarked our results with a fifth strain, a seizure-free wild type (sfWT) *ash1l* strain. In total, after discarding 14 experiments out of 109 (due to experimental disturbances, see Methods), we ended up with 488 time series from seizures, and 661 from background activity (more details in Table I). The number of segmented background events is in general higher than the number of seizures since some anomaly was detected but not confirmed to be an ictal event (see Methods). Note that there are more experiments for the *kcnq5a* fishline, leading to class imbalance: we took this into account in the statistical analysis. More details on the data collection and pre-processing can be found in Methods.

Table I. **Data summary.** For each epileptogenic fishline, either in variant MUT or WT, we report the total number of experiments performed $N_{\text{exp.}}$, the number of experiments discarded from the analysis $N_{\text{drop.}}$ (see Methods). For accepted experiments, $N_{\text{acc.}} = N_{\text{exp.}} - N_{\text{drop.}}$, we report the total number of seizures $N_{\text{seiz.}}$ and background recordings $N_{\text{backgr.}}$, and the mean number of seizures $\langle n_{\text{seiz.}} \rangle = N_{\text{seiz.}}/N_{\text{acc.}}$. Seizure-free strain WT does not have seizures (-) and is denoted sfWT.

Fishline	Cond.	$N_{\text{exp.}}$	$N_{\text{drop.}}$	$N_{\text{seiz.}}$	$N_{\text{backgr.}}$	$\langle n_{\text{seiz.}} \rangle$
ash1l	MUT	20	2	46	54	3.7
ash1l	WT	3	0	20	24	7.3
kcnq5a	MUT	37	11	223	224	8.8
kcnq5a	WT	43	1	56	63	4.0
kcnq5a	sfWT	6	0	-	111	-
Total		109	14	488	661	6.0

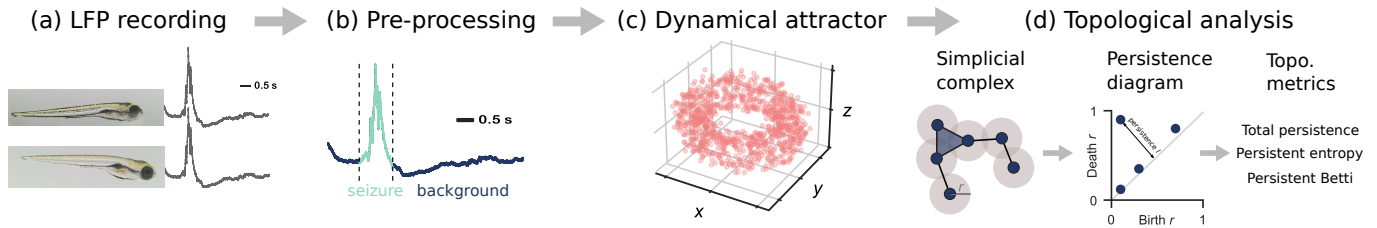


Figure 1. **Analysis pipeline.** (a) We recorded Local Field Potential activity of Zebrafish larvae of two different fishlines. (b) Each raw LFP recording was pre-processed, fed to a Machine Learning classifier for labeling (*i.e.* distinguishing “seizure” and “background”), further confirmed by a trained neuroscientist, and split. (c) From each single-label recording, we reconstructed the associated dynamical attractor using time-delay embedding: the recording is mapped from time series in a suitable higher dimensional space. (d) From each dynamical attractor, we compute a persistence diagram using Topological Data Analysis. From it, we extract three topological metrics: total persistence, persistent entropy and persistent Betti numbers. Finally, we compare the topology of brain activity by comparing these three metrics under different biological conditions: fishline, genetic mutation, and seizure or background activity.

B. Analysis pipeline

The complete analysis pipeline consists of four main steps (Fig. 1): (1) experimental recording of the LFP under different conditions (Fig. 1a), (2) automated pre-processing to classify ictal and non-ictal periods (Fig. 1b-d), (3) characterization of the topology of each recording with TDA (Fig. 1e-h). Finally, (4) we compared the topology under the different conditions to find common patterns (Fig. 1i). Further details can be found in the Methods section.

To analyze the topology of the recorded LFP dynamics, we first need to reconstruct the original higher-dimensional dynamics of the fish brains. To do so, we apply time-delay embedding to each of the time series (see Methods). For each input time series, the method yields multi-variate time series, which mapped into a set of points in a d -dimensional state space, where each point represents the state of the LFP activity at a given time. In dynamical systems terminology, this set of points is a dynamical attractor. We then analyze the topology of each attractor with persistent homology, which outputs persistence diagrams encoding information about the attractors’ topological features and their persistence across scales (*cf.* Methods). We further summarize each persistence diagram by a vector of three topological metrics computed from it: persistent entropy, total persistence, and persistent Betti numbers. Betti numbers measure the connectedness of the attractor by counting its holes; total persistence quantifies the scale at which the attractor is connected, while persistent entropy encodes the information associated with scale invariance (see Methods for a more detailed description). We finally compare these topological metrics and tested if they differed between fishlines, genetic variant, or type of event.

C. Topology of LFP dynamics

To begin with, we assessed that TDA was effective to detect and differentiate topological signatures. In fact, the data-driven reconstruction of LFP state-spaces requires further quantification and systematic categorization to be automatically processed and segmented. TDA is, in principle, an effective method to perform such task, but its statistical power in discriminating seizure events and other topological blueprints still needs assessment.

We thus tested whether there were statistically significant differences in topology by performing a permutation ANOVA with three factors: Fishline (ash11 vs kcnq5a), Condition (mutant vs wild type), and Event (background vs seizure). We did this for each topological metric and each homology dimension separately. For this analysis, we used the complete dataset summarized in Table I except for the seizure-free group (ash11 sfWT). The results are described below and summarized in Table II. Overall, Event was a significant main effect with a large effect size in all cases, whereas Condition and Fishline are main effects (or their interaction is significant) in much fewer cases and with much smaller effect sizes.

First, we examined H_0 , which represents connected components in the attractor. At H_0 , for total persistence, permutation ANOVA indicated that there was no main effect of any of the factors or their pairwise interactions. Only their triple interaction was significant but with a very small effect size ($p = 0.02$, $\eta_p^2 = 0.004$). For both persistent entropy and persistent Betti numbers, the Event factor was the only main effect with a large effect size ($p < 10^{-15}$, $\eta_p^2 = 0.58$). The triple interaction was also significant for both metrics ($p = 0.010$ and $p < 10^{-15}$, respectively), but with very small effect sizes ($\eta_p^2 = 0.007$ and $\eta_p^2 = 0.008$, respectively). This indicates that, at the level of connected components (H_0), the topology differed significantly between background and seizures in two of the three metrics, explaining approximately 60% of the variance in the data. However, the topology did not differ between fishlines or genetic

conditions.

Table II. **Statistical analysis summary.** Significant effects on the topological metrics Total Persistence, Persistent Entropy, and Persistent Betti, determined by a three-way permutation ANOVA with factors Event (background vs seizure), Condition (MUT vs WT), and Fishline (kcnq5a vs ash11), for homological dimensions H_0 and H_1 . We report the p -value associated to each effect, and the effect size measured by partial eta squared η_p^2 .

Metric	Signif. effects	p -value	η_p^2 (%)
H_0			
Total Persistence	Triple Interaction	0.02	0.4
	Persistent Entropy		
Persistent Entropy	Event	$< 10^{-15}$	58.0
	Triple Interaction	0.010	0.7
Persistent Betti			
Persistent Betti	Event	$< 10^{-15}$	58.0
	Triple Interaction	$< 10^{-15}$	0.8
H_1			
Total Persistence			
Total Persistence	Event	$< 10^{-15}$	24.2
	Condition	$< 10^{-15}$	1.4
	Condition:Fishline	0.031	0.5
	Triple Interaction	$< 10^{-15}$	1.3
Persistent Entropy			
Persistent Entropy	Event	$< 10^{-15}$	66.6
	Fishline	0.045	1.3
	Condition:Fishline	0.030	0.6
Persistent Betti			
Persistent Betti	Event	$< 10^{-15}$	74.4
	Fishline	$< 10^{-15}$	2.0
	Condition:Fishline	0.033	0.7
	Triple Interaction	$< 10^{-15}$	1.2

Second, we examined H_1 , which represents cycles or “holes” in the dynamical attractor (like in Fig. 1e). For total persistence, permutation ANOVA indicated a significant main effect for both Event, with a large effect size ($p < 10^{-15}$, $\eta_p^2 = 0.242$), and Condition, but with a small effect size ($p < 10^{-15}$, $\eta_p^2 = 0.014$). There was also a significant Condition:Fishline interaction ($p = 0.031$, $\eta_p^2 = 0.005$) and triple interaction ($p < 10^{-15}$, $\eta_p^2 = 0.013$), both with small effect sizes. For persistent entropy, Event was a significant main effect with a very large effect size ($p < 10^{-15}$, $\eta_p^2 = 0.666$). Fishline was also a significant main effect, but with a small effect size ($p = 0.045$, $\eta_p^2 = 0.013$). The Condition:Fishline interaction was significant, but with a very small effect size ($p = 0.030$, $\eta_p^2 = 0.006$). The results for persistent Betti numbers were similar to those for persistent entropy, as observed for H_0 . Both Event and Fishline were significant main effects ($p < 10^{-15}$ in each case) with a very large effect size for Event ($\eta_p^2 = 0.744$) but a small effect size for

Fishline ($\eta_p^2 = 0.02$). There was again a significant Condition:Fishline interaction ($p = 0.033$, $\eta_p^2 = 0.007$) and a significant triple interaction ($p < 10^{-15}$, $\eta_p^2 = 0.012$), both with small effect sizes. Similarly to H_0 , these results indicate that, at the level of cycles, the topology differs significantly between the background and seizures, explaining between 20% and 75% of the variance in the data, depending on the topological metric. In particular, persistent entropy and the persistent Betti number perform better by explaining substantially more variance from the Event factor, both in H_0 ($\eta_p^2 = 58\%$ vs no main effect) and H_1 ($\eta_p^2 = 66\text{-}75\%$ vs $\eta_p^2 = 24.2\%$).

Overall, these results indicate that the topology of the LFP dynamics is affected by the three biological factors under study (the fishline, the genetic condition, and the type of event) in a complex and intertwined pattern. The topological metrics that we used allow us to uncover this pattern. In the following, we focus on three aspects of these results by performing post hoc analyses.

D. Seizures and background dynamics are topologically different

The strongest signal—by far—in the above analysis is that we can automatically discriminate between seizures and background activity based on the topology of the dynamics, as indicated by the factor Event being a main effect with high variance explained by almost all topological metrics. In Fig. 2, we illustrate this for the mutants of the ash11 fishline : the distribution of topological metrics differ significantly between seizures and background (as shown by pairwise Welch’s t -tests, $p < 10^{-15}$)—except for total persistence in H_0 —and the three topological metrics are consistently higher in background than in seizures. Pairwise Welch’s t -tests yield similar results for the other fishline and genetic mutation, as reported in the Supplementary Material Fig. S1.

Overall, these results confirm that the dynamical attractors associated with “healthy” and “epileptic” activity are altered, irrespective of the underlying biological condition, and that TDA is an appropriate tool to discriminate between them.

E. Different fishlines share common topological features of LFP dynamics under most conditions

A natural next question is whether the topology of the dynamics can allow us to discriminate between fishlines. The answer to this question is not as clearcut as it was in the case of the even type in the previous section. We found that under most biological conditions and topological metrics, the fishlines can not be distinguished. However, going to homological dimension 1 (H_1) and looking at mutants, the fishlines do differ significantly, although with small effect sizes. We detail these results below.

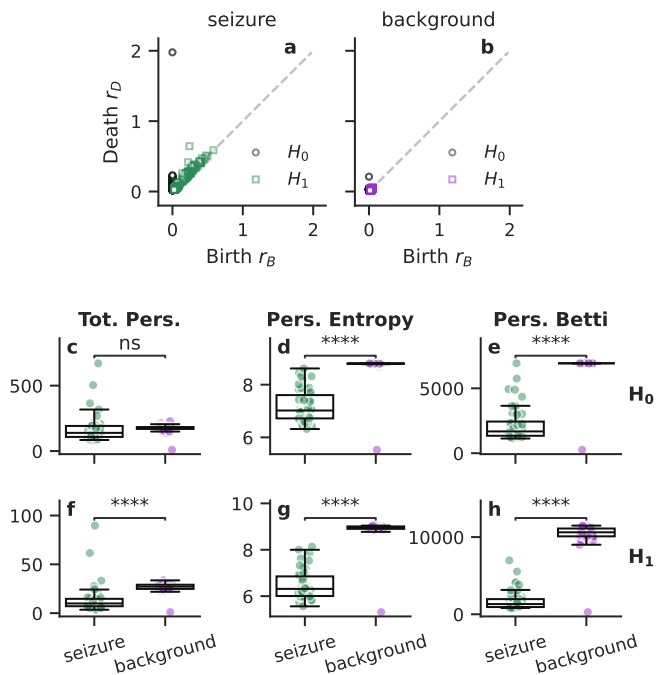


Figure 2. The topology of dynamics discriminates between seizures and background LFP activity. Example persistence diagrams for a mutant of the *ash1l* fishline during (a) seizure and (b) background activity. We show three topological metrics—(a, d) total persistence, (b, e) persistent entropy, and (c, f) persistent Betti—for seizures and background, in homological dimensions (a-c) 0 and (d-f) 1. Pairwise Welch’s *t*-test indicate a significant difference in all cases with $p < 10^{-15}$ (“****”), except for total persistence in H_0 where the difference is not significant (“ns”). Here, results are shown for mutants of the *ash1l* fishline—other fishlines and mutations are reported in Fig. S1.

At the level of connected components, H_0 , none of the topological metrics can discriminate between fishlines—indeed, the permutation ANOVA told us that Fishline was not a main effect. However, at the level of cycles, H_1 , Fishline is a main effect for persistent entropy and the persistent Betti number, and there is an interaction Condition:Fishline, as reported in the last section. To better understand this effect, we performed post hoc analyses in the form of pairwise Welch’s *t*-test between the two fishlines, for each (Condition, Event) subgroup. In Fig. S2, we report that, for seizures, the two fishlines differ only significantly ($p = \dots$) in persistent entropy in MUT, but not in the other two topological metrics, and not in WT. This is a reflection of the Condition:Fishline interaction found by the permutation ANOVA. For background activity, we have a more consistent signal: the two fishlines differ significantly in all three metrics in MUT, but only for total persistence in WT (Fig. 3). In summary, we were able to discriminate between fishlines only under a very specific lens: only from the background activity of the mutants by looking at cycles (H_1)—but not from seizures, not from WT, and not from H_0 .

Overall, being prone, or having developed seizures, make the two genetically different fishlines very close in the topological space, unraveling a shared dynamics at fundamental level.

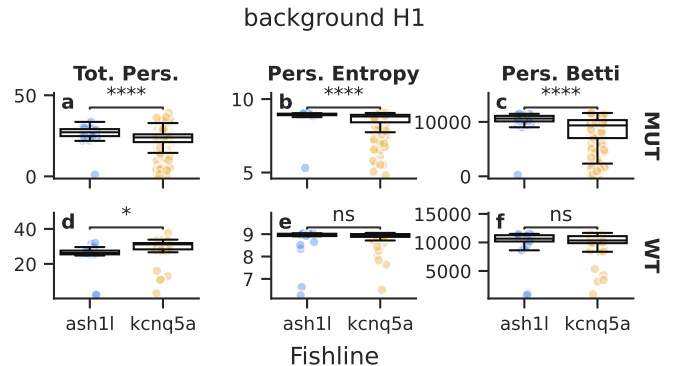


Figure 3. The topology of dynamics can consistently discriminate between fishlines only under a very specific lens: background activity of mutants by looking H_1 . We show three topological metrics—(a, d) total persistence, (b, e) persistent entropy, and (c, f) persistent Betti—for two genetic conditions—MUT and WT. The homological dimension is 1 and we show background activity (see Fig. S2 for seizures). Pairwise Welch’s *t*-test indicate a significant difference in mutants for all three metrics with $p < 10^{-15}$ (“****”). “ns” denotes no significant differences and “*” indicates $10^{-2} < p < 5 \times 10^{-2}$.

F. Detecting seizure-prone specimen from background

Finally, we asked: Is there any topological difference between the background activity of fish that have had seizures and those that have not? Unraveling such differences could help identify early signs of seizure susceptibility based only on LFP signals. To test this, we used the background activity recordings of wild-type *kcnq5a* fishline, and compared two groups: those with seizures (WT) and the seizure-free ones (sfWT) (see Table I).

Figure 4 shows the comparison between these two groups for the three topological metrics for H_0 and H_1 . All three metrics differ significantly between the WT and sfWT groups, as indicated by pairwise Welch’s *t*-tests (all $p < 10^{-7}$) showing large effect sizes (η^2 values between 25-35% for H_0 and between 37-46% for H_1). In all cases, the topological metrics take higher values in WT than in sfWT. The variance of the sfWT group was also significantly larger in all cases as indicated by a pairwise Levene test (Fig. S3). In addition, we observed that the dynamics of the WT and MUT groups were topologically more similar to each other than to the sfWT group (Fig. S4). Surprisingly, this indicates that in this case, having had a seizure affects the topology of the brain activity more than having any mutation. Disruptions in the attractor landscape can thus help differentiating individuals that

have had seizures (and could have others) from the non-epileptic individuals, and that topological markers may complement or even surpass certain biomarkers.

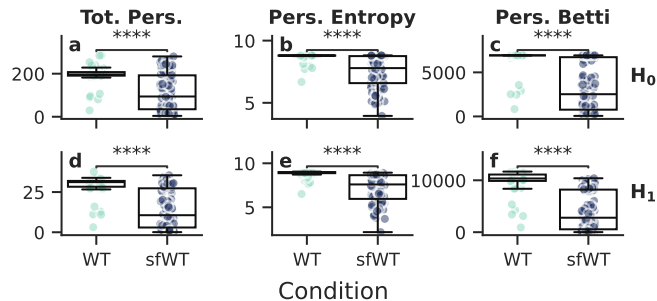


Figure 4. **Wild types with (WT) and without (sfWT) seizures can be discriminated topologically from background LFP dynamics.** We show three topological metrics—total persistence, persistent entropy, and persistent Betti—for two populations of a single fishline (*kcnq5a*): those with and without seizures, in homological dimensions 0 and 1.

III. DISCUSSION

It has been hypothesized that seizures emerge from dynamical landscapes [8, 9] that are altered by neurological and biological conditions [13]. Our study supports this hypothesis by providing a comprehensive and quantitative analysis of seizure dynamics from a controlled experimental dataset of Zebrafish animal models, which allows to precisely characterize the genetic underpinnings of epilepsy. The use of Topological Data Analysis, a stable and powerful method for multiscale analysis of brain dynamics, sheds new insights about the landscape topology emerging from LFP signals. Our results support the use of TDA as an interpretable complement to machine- and deep-learning tools [22] for data-driven detection of epileptic seizures, and unravel that seizures evolve over a dynamical attractor that display altered patterns from those of background activity. On top of the significance for monitoring applications, this observation supports and informs the use of theoretical models to reproduce attractors and bifurcations in brain activity [8, 45].

Our study allows to classify between background and seizure states across fish lines and genetic conditions, and to unravel precursor signatures of seizure susceptibility in Zebrafish larvae. We verify that even different genomic profiles yield similar dynamical blueprints for brain dynamics, which, after processing with TDA, may reveal anticipated susceptibility for seizure states. Our results allow to build a robust and quantitative method to identify similar dynamical states, beyond simple metrics like inter-spike interval, enabling comparison across fish lines and, potentially, across species; moreover, it paves the way to develop screening tools for advanced seizure sensitivity detection.

Our analysis proved to be robust for all fish conditions. The few discarded data series were associated to experimental disturbances, like misplaced needles or off-temperature conditions in the *kcnq5a* fish line, or to uncertain seizure labeling by both the algorithm and the expert. Transitioning to applications on human recordings would require assessing the robustness of persistent topological metrics on LFP and EEG signals, potentially recorded through multiple electrodes. Extraction of TDA signals from LFP has already been performed [26, 27], and future studies may further confirm their use for landscape characterization and seizure precursor detection. Moreover, we extracted TDA metrics from landscapes reconstructed via dynamical embedding from open libraries, which may be sensitive to noise in data. TDA is a robust technique against noise artifacts [15], but new embedding techniques involving noise filtering may further help reducing the observed variability.

Even today, a significant percentage of epileptic patients go unnoticed for long time or do not fully respond to drug treatment [46]. This challenges suggest that our understanding of underlying epileptogenic mechanisms is still limited and can result into poor screening capabilities and a lack of specific diagnoses. Quantitative analysis of seizure susceptibility has the potential to transform the clinical approach towards patients. An accurate signal could provide additional screening capabilities to identify susceptible patients early on and promptly initiate treatment. In addition, it may help forecasting states close to seizure onsets, triggering warnings and interventions. Integrating multi-faceted approaches [47, 48] for quantifying seizure risks, building on automated TDA-based assessment of seizure precursors and potentially embedded in portable devices [49], has the potential to improve the long-term monitoring and treatment of people living with epilepsy.

IV. METHODS

The analysis pipelines involves several steps (Fig. 1): data collection (from published datasets or from new experiments), data processing for topological data analysis (which includes preprocessing of raw signals, including anomaly detection, automated time series segmentation into background and seizure events, time-delay embedding to reconstruct topological information using dynamical attractors, and TDA), and statistical analysis on TDA results. Each step is detailed in the subsections below.

A. Data collection

The time series data was generated by measuring Local Field Potential (LFP) recordings in zebrafish (*Danio rerio*) larvae from a KCNQ5 LoF model *kcnq5a*^{sa9563} ze-

brafish and the ASH1L model ash11^{sa19097} obtained from ZFIN repository.

1. Ethics statement

Zebrafish were handled as described previously in [50, 51] at the Luxembourg Centre for Systems Biomedicine (LCSB). The Aquatic Facility at the LCSB is registered as an authorized breeder, supplier, and user of zebrafish by the relevant agency of the Government of Luxembourg (Ministry of Agriculture, Viticulture and Rural Development). Experiments using zebrafish larvae at 5 days post-fertilization were performed under Grand-Ducal decrees. All practices involving zebrafish were performed in accordance with European laws, guidelines and policies for animal experimentation, housing, and care (European Directive 2010/63/EU on the protection of animals used for scientific purposes) and following the principles of the Three Rs. Furthermore, we carefully comply with ARRIVE guidelines.

2. Zebrafish husbandry

Adult zebrafish were maintained in the Aquatic Facility of the Luxembourg Centre for Systems Biomedicine and housed at 28.5 °C in a 14-h/10-h light/dark cycle according to standard protocols. Embryos were obtained by natural spawning and fertilized eggs were selected and raised at 28 °C in 0.3X Danieau’s medium (17 mM NaCl, 2 mM KCl, 0.12 mM MgSO₄, 1.8 mM Ca(NO₃)₂, 1.5 mM HEPES pH 7.5 and 1.2 μM methylene blue). Developmental staging was accessed by following standard procedure [52] and larvae were used used 5 days post fertilization (dpf) for experiments. The corresponding genotype (WT vs heterozygous and homozygous) was accessed by a posteriori sequencing of the corresponding genes *kcnq5a* and *ash11*, respectively. For the analysis, we use homozygous mutants (MUT).

3. Local field potential recordings

LFP were performed as previously described in [51]. In brief, each 5 dpf larva was placed in a 50 μL of Danieau’s medium in the recording chamber with a transfer pipette, and then 200 μL of 2% low melting point agar were added. The chamber was transferred on the stage of a stereomicroscope for LFP recordings of a full electrophysiology system (Scientifica SliceScope Pro 1000) equipped with a MultiClamp 700B amplifier and Digidata 1550 A digitizer (Axon instruments, USA). The local field potential (LFP) was recorded at 100 kHz in current clamp mode by a glass microelectrode (4–10 MΩ resistance) back loaded with extracellular recording solution and placed under visual guidance in the medial tectal band of the midbrain.

4. Dataset

The resulting dataset is a collection of time series for brain activity, along with information about the fishline and information on the mutation type (WT, heterozygous and homozygous). The full data set was first parsed to look for warnings about experimental issues or potential bias, such as electrodes not being well-placed or signals looking altered. This initial pre-processing resulted in a few dropouts for each fishline (Table I).

B. Data segmentation and labeling

The original local field potential (LFP) signal was downsampled from 100kHz to 2000Hz, discarding frequencies higher than 2000Hz which are usually associated with random noise instead of biologically relevant brain dynamics. Then, the 50Hz signal artifact was removed with a notch filter.

The downsampled recording was then analysed with an automated anomaly detection pipeline. For this, the signal was first decomposed into 11 sub-frequency ranges, through a multi-resolution analysis using the Maximal Overlap Discrete Wavelet Transform (MODWT) and a Daubechie 4 (db4) wavelet. Wavelet Transforms overcome the main limitation of the Fourier Transform. The latter characterizes the original signal in the frequency domain but loses information on the all-time domain; instead, Wavelet Transform creates a representation of the signal in the time and frequency domain, which allows the localization of time-dependent information in the signal. The MODWT is a non-decimating wavelet transform that does not downsample the signal at each scale during processing and produces time-aligned signals. This allows for a straightforward correlation between events in the original signal and in each extracted signal for all sub-frequency ranges. Daubechie 4 wavelets have two vanishing moments, easily encode second-order polynomials, and are widely used to cope with signal discontinuities [53]. The 11 sub-frequency ranges were [1000-2000]Hz, [500-1000]Hz, [250-500]Hz, [125-250]Hz, [62-125]Hz, [31-62]Hz (gamma waves), [16-31]Hz (beta waves), [8-16]Hz (alpha waves), [4-8]Hz (theta waves), [2-4]Hz (high delta waves) and [0-2]Hz (low delta waves).

These decomposed signals were then fed to the anomaly detection algorithm, which applies an amplitude threshold in the [62-125]Hz, [31-62]Hz, and [16-31]Hz sub-frequency ranges, as well as a temporal threshold, to select and extract all seizure candidates. To detect anomalous signals, the algorithm applies a threshold to select only the data points above the 95th percentile as well as a contiguity threshold which filters all anomalies occurring for less than a second. The amplitude threshold is applied to each targeted sub-frequency range, the temporal threshold is applied to all data points selected through the amplitude threshold in the three sub-frequency ranges simultaneously.

This processed helped to automatize the process and to provisionally assign a "seizure" labeling to anomalies. Background segments resulted from the time series cropped between anomalies. After extraction, all candidates were submitted for expert evaluation to produce labels identifying anomalies or seizures. Some anomalies did not pass the expert judgment and were discarded from the seizure set. In these cases, segmented background time series were not artificially collated but were kept separate to prevent artifacts.

C. Time-delay embedding

Pre-processing and segmentation yield a set of univariate timeseries, with an additional label corresponding to the type of event (background or seizure). Each time series then passed for analysis corresponds to the processed measurement of the electrical activity of a certain fish $f_i \in F$, belonging to one fish line $l_j \in L$, during a given event $e_k \in E$. Hence, each post-processed time series can be considered as an element $a_{i,j,k}$ of the tensor dataset $A = F \times L \times E$.

To analyze the dynamics of each $a_{i,j,k}$, we use a standard technique from dynamical systems theory: *time-delay embedding*. The method has its theoretical grounds in Takens' theorem [24], which provides the conditions to reconstruct a smooth attractor from observations made with generic functions. Its application is motivated by interpreting the fish's brain activity as a high-dimensional dynamical systems, of which the one-dimensional time series is a partial observation. The time-delay embedding allows us, to a certain extent, to reconstruct the full attractor associated with the fish' brain dynamics.

In practice, given discrete time series (like the ones obtained from measurements) $\{x_0, x_1, \dots\}$, and evenly sampled time sequences $\{t_0, t_1, \dots\}$, the result of the embedding is a set of vectors in a d -dimensional state space, $X = \{x_{t_i}, x_{t_i+\tau}, \dots, x_{t_i+(d-1)\tau}\}$, with $i = 0, 1, \dots$. Each data point in X represents the state of the reconstructed brain dynamics in d dimensions at a given time. For example, processing the time series of a sinusoidal oscillation with time-delay embedding results in points forming a circle in a 2-dimensional space. Hence, the shape of the final embedding contains information about the type of dynamics considered and allows functional observability of dynamical systems [54].

The method involves two parameters: the delay τ , and the embedding dimension d . Both parameters are determined using standard techniques [24, 55] implemented in the Python toolbox `giotto-tda` [56]. The same toolbox is then used to determine the time-delay embedding of each processed time series.

D. Topological data analysis

Topological data analysis as a field employs concepts from topology to analyze data. Topology provides mathematical tools to study and compare the shape properties of objects (or data), like connected components, and holes in different dimensions. It thus extract the topological bases of each shape, similarly to using basis vectors and corresponding rank to compare the structure of matrices [44]. A visual example is that of a donut, which is topologically equivalent to a mug because both display one hole. TDA allows to study topological properties in clouds of data points, sampled from dynamical attractors. In particular, the *persistent homology* [57, 58] technique quantitatively describes the existence, or persistence, of these holes across several spatial resolution scales, and is robust against noise in the data.

Computing persistent homology consists of two main steps. First, it connects data points to form a *simplicial complex*, a mathematical object which generalises the notion of graphs [59]. Simplicial complexes are defined as a set of nodes – the data points – and a set of simplices, which represent the connections between two or more nodes. For example, a simplex connecting nodes 1, 2, and 3 can be regarded as a $\{1, 2, 3\}$ object. This step is usually performed with the Vietoris-Rips process [60]: after embedding data points in a suitable space, and given a set of radii $\{r_1, r_2, \dots\}$ generating balls $\{\mathcal{B}(r_1), \mathcal{B}(r_2), \dots\}$ around each data point, the procedure connects the nodes whose balls $\mathcal{B}(r_m)$ intersect. Each radius r_m corresponds to a resolution scale for analysis: for a very small r_m , none of the points will be connected, whereas a large r_m guarantees that all nodes are connected with all the others. Persistent homology is a multi-scale tool which creates a set of simplicial complexes, each one corresponding to a certain r_m .

Then, the persistent homology pipeline outputs a barcode diagram, or equivalently a persistence diagram [61], which describes the data topology over the resolution scales. Both diagrams encode the radii at which a given-dimensional hole persists, marking the "birth" radius r_B and "death" radius r_D (respectively, the first and last radius that determine a simplicial endowed with a certain hole). The dimension of homology H_n counts the number of n -dimensional holes: H_0 correspond to the number of connected components, H_1 count the number of empty circles (like in the donut case), H_2 counts the number of empty spheres, and so on. Here, we focus on H_0 and H_1 . Holes with a longer "lifetime", that is, more persistent across scales, are typically considered more important, whereas those with short lifetimes are considered noise.

Finally, each persistence diagram obtained by the procedure above is summarised by extracting three topological metric: persistent entropy, total persistence, and persistent Betti numbers. For a persistence diagram $D = \{(r_{B_n}, r_{D_n})\}_{n \in N}$, with $r_{D_n} < \infty$, the persistence

entropy is defined as

$$E(D) = - \sum_{n \in N} p_n \log(p_n), \quad (1)$$

where $p_n = (r_{D_n} - r_{B_n})/L_D$. Here, $L_D = \sum_{n \in N} (r_{D_n} - r_{B_n})$ is the total persistence. Intuitively, Eq. 1 is a measure of the entropy of each point in the diagram. The Betti number β_n counts the number of unique n -holes in a simplex. It can be seen as the total number of unique topological features. While persistent Betti numbers and total persistence are arguably more well-known [62], we also employ persistent entropy since it is stable, scale invariant and more robust to noise [63].

In the present analysis, we apply persistent homology on the data clouds generated by time-delay embedding, and use all three topological measures. For this task, we use functions from the `giotto-tda` Python package [56].

E. Statistical analysis

Permutation analyses of variance (ANOVAs) performed and permutation t -tests were all performed with the standard value of permutations (5000 vs 9999, respectively), unless otherwise stated. Posthoc analysis was performed when applicable with pairwise Welch's t -tests, and Bonferroni-corrected when applicable.

ACKNOWLEDGMENTS

The authors would like to thank the Aquatic Platform of the LCSB for excellent animal handling. M.L. is a Postdoctoral Researcher of the Fonds de la Recherche Scientifique-FNRS. C.D. and A.S.'s work

was supported by the Luxembourg National Research Fund (FNR) through INTER/DFG/17/11583046 and the Caisse Médico-Complémentaire Mutualiste Luxembourg (CMCM) fellowship for C.D. in the framework of the Luxembourg National Research Fond (FNR) PRIDE DTU CriTiCS (grant reference 10907093). A.S. and D.F. acknowledge financial support of the Institute for Advanced Studies of the University of Luxembourg through an Audacity Grant (IDAE-2020). D.P. was partially funded by the European Union through the ERC INSPIRE grant (project number 101076926). Views and opinions expressed are however those of the author only and do not necessarily reflect those of the European Union or the European Research Council. Neither the European Union nor the granting authority can be held responsible for them.

AUTHOR CONTRIBUTIONS

Conceived and designed the work: D.P., M.L., A.S. Collected and curated data: C.D., D.F., A.S., D.P. Developed software and performed computational analysis: M.L., D.F. Interpreted results: D.P., M.L., D.F., A.S. Supervised the project: D.P., A.S. Wrote the paper: D.P., M.L., D.F., A.S.

COMPETING INTERESTS

The authors declare no competing interests.

DATA AVAILABILITY

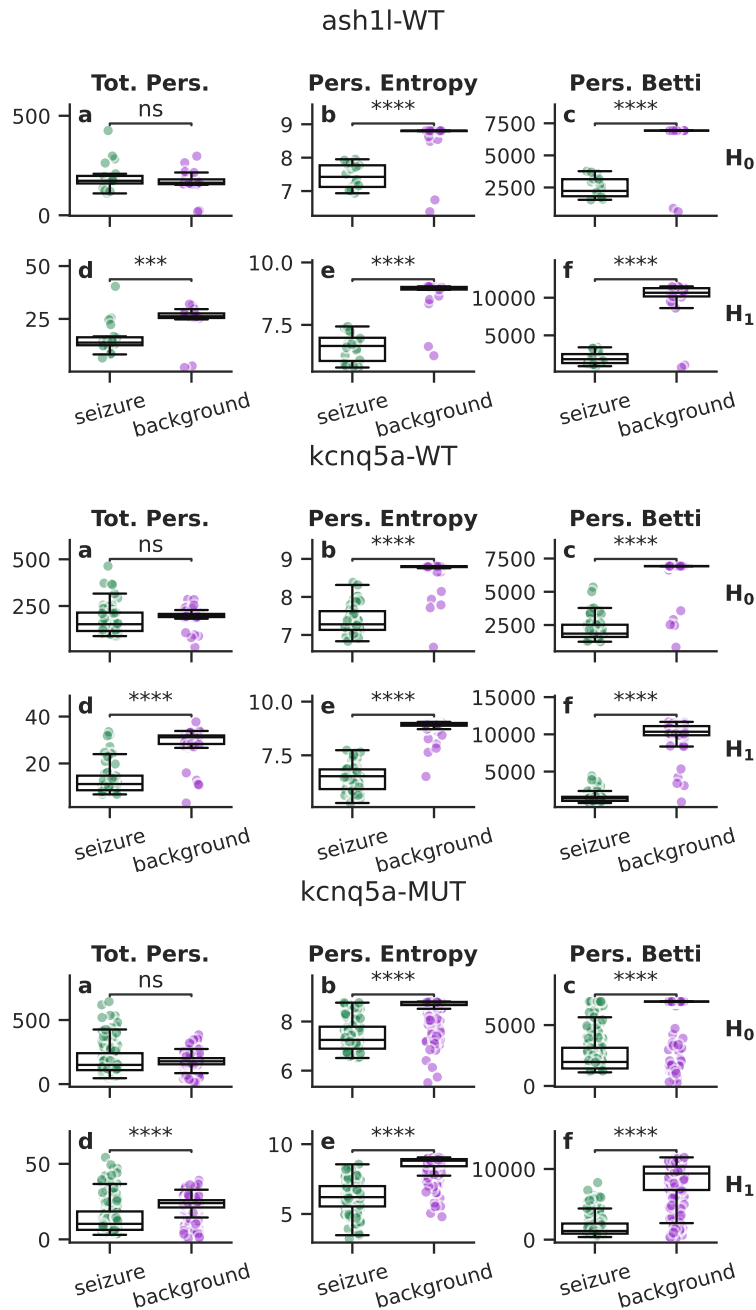
Original data are available upon request.

-
- [1] W. H. Organization, Epilepsy, <https://www.who.int/news-room/fact-sheets/detail/epilepsy>, accessed: 2024-12-01.
- [2] R. G. Andrzejak, H. P. Zaveri, A. Schulze-Bonhage, M. G. Leguia, W. C. Stacey, M. P. Richardson, L. Kuhlmann, and K. Lehnertz, Seizure forecasting: Where do we stand?, *Epilepsia* **64**, S62 (2023).
- [3] K. Rasheed, A. Qayyum, J. Qadir, S. Sivathamboo, P. Kwan, L. Kuhlmann, T. O'Brien, and A. Razi, Machine learning for predicting epileptic seizures using eeg signals: A review, *IEEE Reviews in Biomedical Engineering* **14**, 139 (2020).
- [4] V. K. Jirsa, W. C. Stacey, P. P. Quilichini, A. I. Ivanov, and C. Bernard, On the nature of seizure dynamics, *Brain* **137**, 2210 (2014).
- [5] M. G. Leguia, R. G. Andrzejak, C. Rummel, J. M. Fan, E. A. Mirro, T. K. Tcheng, V. R. Rao, and M. O. Baud, Seizure Cycles in Focal Epilepsy, *JAMA Neurology* **78**, 454 (2021).
- [6] P. Perucca, M. Bahlo, and S. F. Berkovic, The Genetics of Epilepsy, *Annual Review of Genomics and Human Genetics* **21**, 205 (2020).
- [7] S. H. Strogatz, *Nonlinear Dynamics and Chaos: With Applications to Physics, Biology, Chemistry, and Engineering*, 2nd ed. (Westview Press, Boulder, 2014).
- [8] M. Breakspear, Dynamic models of large-scale brain activity, *Nature neuroscience* **20**, 340 (2017).
- [9] F. Freyer, K. Aquino, P. A. Robinson, P. Ritter, and M. Breakspear, Bistability and non-gaussian fluctuations in spontaneous cortical activity, *Journal of Neuroscience* **29**, 8512 (2009).
- [10] D. Proverbio, A. Skupin, and J. Gonçalves, Systematic analysis and optimization of early warning signals for critical transitions using distribution data, *Iscience* **26** (2023).
- [11] D. Proverbio, R. Katz, and G. Giordano, Bridging robustness and resilience for dynamical systems in nature, *IFAC-PapersOnLine* **58**, 43 (2024).

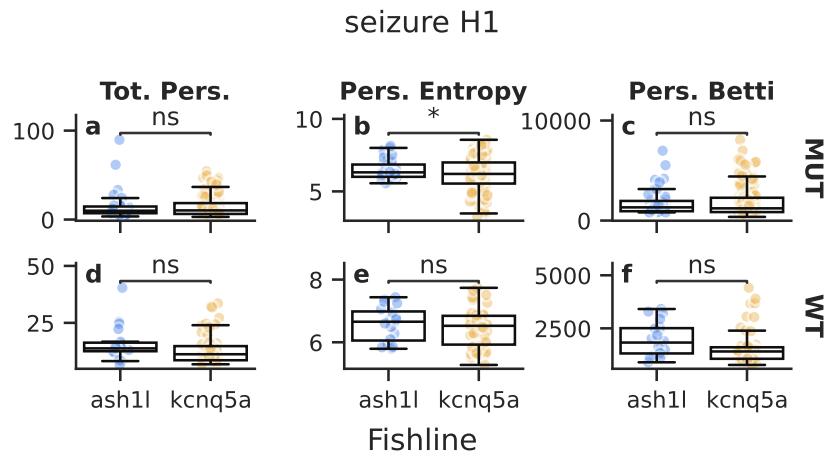
- [12] H. Chu, C. K. Chung, W. Jeong, and K.-H. Cho, Predicting epileptic seizures from scalp eeg based on attractor state analysis, *Computer methods and programs in biomedicine* **143**, 75 (2017).
- [13] F. H. L. da Silva, W. Blanes, S. N. Kalitzin, J. Parra, P. Suffczynski, and D. N. Velis, Dynamical diseases of brain systems: different routes to epileptic seizures, *IEEE transactions on biomedical engineering* **50**, 540 (2003).
- [14] M. Breakspear, J. A. Roberts, J. R. Terry, S. Rodrigues, N. Mahant, and P. A. Robinson, A unifying explanation of primary generalized seizures through nonlinear brain modeling and bifurcation analysis, *Cerebral Cortex* **16**, 1296 (2006).
- [15] N. Atienza, R. Gonzalez-Diaz, and M. Rucco, Separating topological noise from features using persistent entropy, in *Federation of International Conferences on Software Technologies: Applications and Foundations* (Springer, 2016) pp. 3–12.
- [16] P. Expert, L.-D. Lord, M. L. Kringelbach, and G. Petri, *Topological neuroscience* (2019).
- [17] K. Benjamin, A. Bhandari, J. D. Kepple, R. Qi, Z. Shang, Y. Xing, Y. An, N. Zhang, Y. Hou, T. L. Crockford, *et al.*, Multiscale topology classifies cells in subcellular spatial transcriptomics, *Nature*, 1 (2024).
- [18] X. Xu, N. Drougard, and R. N. Roy, Topological data analysis as a new tool for eeg processing, *Frontiers in Neuroscience* **15**, 761703 (2021).
- [19] H. Osterhage and K. Lehnertz, Nonlinear time series analysis in epilepsy, *International Journal of Bifurcation and Chaos* **17**, 3305 (2007).
- [20] M. I. Maturana, C. Meisel, K. Dell, P. J. Karoly, W. D'Souza, D. B. Grayden, A. N. Burkitt, P. Jiruska, J. Kudlacek, J. Hlinka, *et al.*, Critical slowing down as a biomarker for seizure susceptibility, *Nature communications* **11**, 2172 (2020).
- [21] T. Wilkat, T. Rings, and K. Lehnertz, No evidence for critical slowing down prior to human epileptic seizures, *Chaos: An Interdisciplinary Journal of Nonlinear Science* **29**, <https://doi.org/10.1063/1.5122759> (2019).
- [22] M. K. Siddiqui, R. Morales-Menendez, X. Huang, and N. Hussain, A review of epileptic seizure detection using machine learning classifiers, *Brain informatics* **7**, 1 (2020).
- [23] X. Ding, W. Nie, X. Liu, X. Wang, and Q. Yuan, Compact convolutional neural network with multi-headed attention mechanism for seizure prediction, *International Journal of Neural Systems* **33**, 2350014 (2023).
- [24] F. Takens, Dynamical systems and turbulence, *Warwick*, 1980, 366 (1981).
- [25] Y. Wang, H. Ombao, and M. K. Chung, Topological data analysis of single-trial electroencephalographic signals, *Annals of Applied Statistics* **12**, 1506 (2018).
- [26] E. Merelli, M. Piangerelli, M. Rucco, and D. Toller, A topological approach for multivariate time series characterization: The epileptic brain, *EAI International Conference on Bio-inspired Information and Communications Technologies (BICT)*, 5 (2015).
- [27] M. Piangerelli, M. Rucco, L. Tesei, and E. Merelli, Topological classifier for detecting the emergence of epileptic seizures, *BMC Research Notes* **11**, 10.1186/s13104-018-3482-7 (2018).
- [28] Y. Ren, F. Liu, S. Xia, S. Shi, L. Chen, and Z. Wang, Dynamic eeg signal quality evaluation based on persistent homology and googlenet method, *Frontiers in Neuroscience* **17**, 1153386 (2023).
- [29] X. Fernández and D. Mateos, Topological biomarkers for real-time detection of epileptic seizures, arXiv preprint arXiv:2211.02523 <https://doi.org/10.48550/arXiv.2211.02523> (2022).
- [30] G. Petri, P. Expert, F. Turkheimer, R. Carhart-Harris, D. Nutt, P. J. Hellyer, and F. Vaccarino, Homological scaffolds of brain functional networks, *Journal of The Royal Society Interface* **11**, 20140873 (2014).
- [31] J. Billings, M. Saggat, J. Hlinka, S. Keilholz, and G. Petri, Simplicial and topological descriptions of human brain dynamics, *Network Neuroscience* **5**, 549 (2021).
- [32] E. Ibáñez-Marcelo, L. Campioni, A. Phinyomark, G. Petri, and E. L. Santarcangelo, Topology highlights mesoscopic functional equivalence between imagery and perception: The case of hypnotizability, *NeuroImage* **200**, 437 (2019).
- [33] A. Karan and A. Kaygun, Time series classification via topological data analysis, *Expert Systems with Applications* **183**, 115326 (2021).
- [34] M. Gidea and Y. Katz, Topological data analysis of financial time series: Landscapes of crashes, *Physica A: Statistical Mechanics and its Applications* **491**, 820 (2018).
- [35] S. Emrani, T. Gentimis, and H. Krim, Persistent homology of delay embeddings and its application to wheeze detection, *IEEE Signal Processing Letters* **21**, 459 (2014).
- [36] M. Piangerelli, M. Rucco, L. Tesei, and E. Merelli, Topological classifier for detecting the emergence of epileptic seizures, *BMC Research Notes* **11**, 392 (2018).
- [37] B. P. Grone and S. C. Baraban, Animal models in epilepsy research: Legacies and new directions, *Nature Neuroscience* **18**, 339 (2015).
- [38] O. Devinsky, J. M. Boesch, S. Cerda-Gonzalez, B. Coffey, K. Davis, D. Friedman, B. Hainline, K. Houpt, D. Lieberman, P. Perry, *et al.*, A cross-species approach to disorders affecting brain and behaviour, *Nature Reviews Neurology* **14**, 677 (2018).
- [39] D. Barkmeier and J. Loeb, An animal model to study the clinical significance of interictal spiking, *Clinical EEG and neuroscience* **40**, 234 (2009).
- [40] L. Wei, H. Boutouil, R. R. Gerbatin, O. Mamad, M. Heiland, C. R. Reschke, F. Del Gallo, P. F. Fabene, D. C. Henshall, M. Lowery, *et al.*, Detection of spontaneous seizures in eegs in multiple experimental mouse models of epilepsy, *Journal of Neural Engineering* **18**, 056060 (2021).
- [41] B. Hunyadi, A. Siekierska, J. Sourbron, D. Copmans, and P. A. de Witte, Automated analysis of brain activity for seizure detection in zebrafish models of epilepsy, *Journal of Neuroscience Methods* **287**, 13 (2017).
- [42] B. D. Fontana, N. J. Mezzomo, A. V. Kalueff, and D. B. Rosemberg, The developing utility of zebrafish models of neurological and neuropsychiatric disorders: A critical review, *Experimental neurology* **299**, 157 (2018).
- [43] V. T. Cunliffe, R. A. Baines, C. N. Giachello, W.-H. Lin, A. Morgan, M. Reuber, C. Russell, M. C. Walker, and R. S. Williams, Epilepsy research methods update: Understanding the causes of epileptic seizures and identifying new treatments using non-mammalian model organisms, *Seizure* **24**, 44 (2015).
- [44] A. D. Smith, P. Dłotko, and V. M. Zavala, Topological data analysis: concepts, computation, and applications in chemical engineering, *Computers & Chemical Engi-*

- neering **146**, 107202 (2021).
- [45] V. K. Jirsa, T. Proix, D. Perdikis, M. M. Woodman, H. Wang, J. Gonzalez-Martinez, C. Bernard, C. Bénar, M. Guye, P. Chauvel, *et al.*, The virtual epileptic patient: individualized whole-brain models of epilepsy spread, *Neuroimage* **145**, 377 (2017).
- [46] W. Löscher, H. Potschka, S. M. Sisodiya, and A. Vezzani, Drug resistance in epilepsy: clinical impact, potential mechanisms, and new innovative treatment options, *Pharmacological reviews* **72**, 606 (2020).
- [47] M. O. Baud, J. K. Kleen, E. A. Mirro, J. C. Andrechak, D. King-Stephens, E. F. Chang, and V. R. Rao, Multi-day rhythms modulate seizure risk in epilepsy, *Nature communications* **9**, 88 (2018).
- [48] E. Krook-Magnuson, C. Armstrong, M. Oijala, and I. Soltesz, On-demand optogenetic control of spontaneous seizures in temporal lobe epilepsy, *Nature communications* **4**, 1376 (2013).
- [49] B. H. Brinkmann, P. J. Karoly, E. S. Nurse, S. B. Dumanis, M. Nasser, P. F. Viana, A. Schulze-Bonhage, D. R. Freestone, G. Worrell, M. P. Richardson, *et al.*, Seizure diaries and forecasting with wearables: epilepsy monitoring outside the clinic, *Frontiers in Neurology* **12**, 690404 (2021).
- [50] M. Moein, K. Grzyb, T. Gonçalves Martins, S. Komoto, F. Peri, A. D. Crawford, A. Fouquier d’Herouel, and A. Skupin, CaSiAn: a Calcium Signaling Analyzer tool, *Bioinformatics* **34**, 3052 (2018).
- [51] T. G. Martins, R. Soliman, M. L. Cordero-Maldonado, C. Donato, C. Ameli, L. Mombaerts, A. Skupin, F. Peri, and A. D. Crawford, Seizure-induced increase in microglial cell population in the developing zebrafish brain, *Epilepsy Research* **195**, 107203 (2023).
- [52] C. B. Kimmel, W. W. Ballard, S. R. Kimmel, B. Ullmann, and T. F. Schilling, Stages of embryonic development of the zebrafish, *Developmental dynamics* **203**, 253 (1995).
- [53] C. Vonesch, T. Blu, and M. Unser, Generalized daubechies wavelet families, *IEEE transactions on signal processing* **55**, 4415 (2007).
- [54] A. N. Montanari, L. Freitas, D. Proverbio, and J. Gonçalves, Functional observability and subspace reconstruction in nonlinear systems, *Physical Review Research* **4**, 043195 (2022).
- [55] M. B. Kennel, R. Brown, and H. D. Abarbanel, Determining embedding dimension for phase-space reconstruction using a geometrical construction, *Physical review A* **45**, 3403 (1992).
- [56] G. Tauzin, U. Lupo, L. Tunstall, J. B. Pérez, M. Caorsi, A. M. Medina-Mardones, A. Dassatti, and K. Hess, giotto-tda: A topological data analysis toolkit for machine learning and data exploration, *Journal of Machine Learning Research* **22**, 1 (2021).
- [57] Edelsbrunner, Letscher, and Zomorodian, Topological persistence and simplification, *Discrete & Computational Geometry* **28**, 511 (2002).
- [58] U. Fugacci, S. Scaramuccia, F. Iuricich, L. De Florian, *et al.*, Persistent homology: a step-by-step introduction for newcomers., in *STAG* (2016) pp. 1–10.
- [59] V. Salnikov, D. Cassese, and R. Lambiotte, Simplicial complexes and complex systems, *European Journal of Physics* **40**, 014001 (2018).
- [60] E. Carlsson, G. Carlsson, and V. De Silva, An algebraic topological method for feature identification, *International Journal of Computational Geometry & Applications* **16**, 291 (2006).
- [61] A. Zomorodian and G. Carlsson, Computing persistent homology, in *Proceedings of the twentieth annual symposium on Computational geometry* (2004) pp. 347–356.
- [62] A. Cerri, B. D. Fabio, M. Ferri, P. Frosini, and C. Landi, Betti numbers in multidimensional persistent homology are stable functions, *Mathematical Methods in the Applied Sciences* **36**, 1543 (2013).
- [63] N. Atienza, R. González-Díaz, and M. Soriano-Trigueros, On the stability of persistent entropy and new summary functions for topological data analysis, *Pattern Recognition* **107**, 107509 (2020).

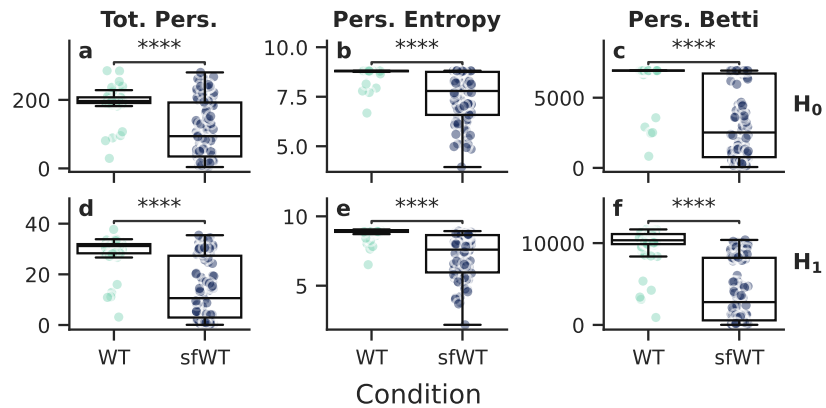
Supplementary Information



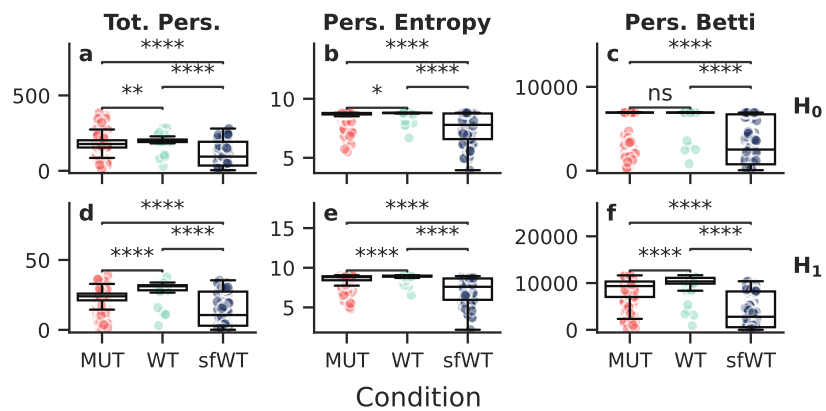
Supplementary Figure S1. **The topology of dynamics discriminates between seizures and background LFP activity.** In complement to Fig. 2, here we show three more subgroups: (ash1l, WT), (kcnq5a-WT), and (kcnq5a-MUT). In each case, we show three topological metrics—(a, d) total persistence, (b, e) persistent entropy, and (c, f) persistent Betti—for seizures and background, in homological dimensions (a-c) 0 and (d-f) 1. Pairwise Welch’s *t*-test indicate a significant difference in all cases with $p < 10^{-15}$ (“****”), except for total persistence in H_0 where the difference is not significant (“ns”).



Supplementary Figure S2. **Different fishlines display similar topological patterns at H_0 but can be discriminated from background at H_1 .** We show three topological metrics—total persistence, persistent entropy, and persistent Betti—for two fishlines—ash1l and kcnq5a—in homological dimensions 0 and 1. Pairwise Welch’s t -test indicate no significant (“ns”) difference in H_0 but persistent entropy and persistent Betti significantly differ between fishlines (“***”).



Supplementary Figure S3. Same figure as Fig. 4, but showing the results of pairwise Levene tests, indicating that the sfWT group has significantly larger variance, with $p < 10^{-15}$ (“****”).



Supplementary Figure S4. Same figure as Fig. 4, but here we add the MUT group.